Supplement of Atmos. Chem. Phys., 18, 6293–6315, 2018
https://doi.org/10.5194/acp-18-6293-2018-supplement

Atmospheric Chemistry and Physics
Open Access
EGU

Supplement of

Low levels of nitryl chloride at ground level: nocturnal nitrogen oxides in the Lower Fraser Valley of British Columbia

Hans D. Osthoff et al.

Correspondence to: Hans D. Osthoff (hosthoff@ucalgary.ca)

15 **Table of contents**

16

Table S-1. Volatile organic compounds quantified by GC-MS

Butane, 2-methyl-	Cyclohexane, methyl-	Benzene, 1,2,3-trimethyl-
1-Pentene	Pentane, 2,3,4-trimethyl-	Benzene, 1,3-diethyl-
Pentane	Heptane, 2-methyl-	Benzene, 1,4-diethyl-
2-Pentene (Z) (cis)	Heptane, 3-methyl-	Undecane
Isoprene (1,3-Butadiene, 2-methyl-)	Toluene	Dodecane
2-Pentene (E) (trans)	Octane	Ethylene
Butane, 2,2-dimethyl-	Ethylbenzene	Acetylene
Cyclopentane	m & p-Xylene	Ethane
2,3-Dimethylbutane	Nonane	Propane
Pentane, 2-methyl-	Styrene	Propylene
Pentane, 3-methyl-	o-Xylene	Isobutane
1-Hexene	Isopropyl Benzene (Benzene, (1-methyleth	1-Butene
Hexane	Benzene, propyl-	Butane
Cyclopentane, methyl-	Benzene, 1-ethyl-3-methyl-	2-Butene (trans)
Pentane, 2,4-dimethyl-	Benzene, 1-ethyl-4-methyl-	2-Butene (cis)
Cyclohexane	Benzene, 1,3,5-trimethyl-	Freon 11 (Trichloromonofluoromethane)
Hexane, 2-methyl-	Decane	Isopropyl Alcohol
Benzene	Benzene, 1-ethyl-2-methyl-	Acetone
2,3-Dimethylpentane	Benzene, 1,2,4-trimethyl-	Ethene, 1,1-dichloro-
Hexane, 3-methyl-		Methylene Chloride
Pentane, 2,2,4-trimethyl-		Freon 113 (Ethane, 1,1,2-trichloro-1,2,2
Heptane		

Carbon disulfide	Methyl Methacrylate	Benzene, 1,4-dichloro-
Ethene, 1,2-dichloro-, (E)-	1-Propene, 1,3-dichloro-, (Z)-	Benzene, 1,2-dichloro-
Methyl tertbutylether (Propane, 2-methox	Methyl Isobutyl Ketone	Benzene, 1,2,4-trichloro-
Ethane, 1,1-dichloro-	1-Propene, 1,3-dichloro-, (E)-	1,3-Butadiene, 1,1,2,3,4,4-hexachloro-
Vinyl Acetate (Acetic acid ethenyl ester	Ethane, 1,1,2-trichloro-	Naphthalene
2-Butanone	2-Hexanone	Freon 12
Chloroform (Trichloromethane)	Methane, dibromochloro-	Chloromethane
Ethyl Acetate	Ethane, 1,2-dibromo-	Freon 114
Furan, tetrahydro-	Tetrachloroethylene	Vinyl chloride
Ethane, 1,2-dichloro-	Benzene, chloro-	1,3 Butadiene
Ethane, 1,1,1-trichloro-	Bromoform (Methane, tribromo-)	Bromomethane
Carbon Tetrachloride	Ethane, 1,1,2,2-tetrachloro-	Chloroethane
Trichloroethylene	Ethane, pentachloro-	Ethanol
Methane, bromodichloro-	Benzyl Chloride	1R-alpha-Pinene
1,4-Dioxane	Benzene, 1,3-dichloro-	Camphene
		beta-Pinene
		D-Limonene

37

38

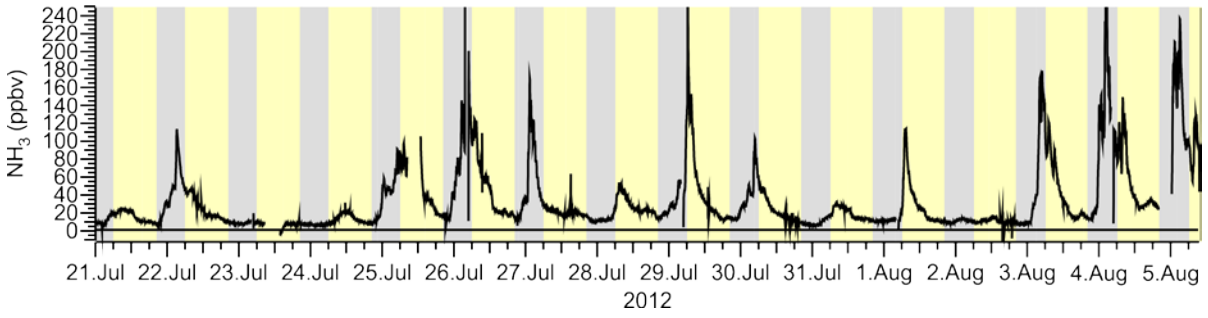

Figure S-1. Time series of gas-phase ammonia data reported by Metro Vancouver. Data were not quality-assured and are non-quantitative.

Box model to rationalize O_x loss by dry deposition

A box model was set up to simulate the median nocturnal decays of O_3 and O_x. These simulations are intended as back-of-the-envelope type estimates of major processes only since an accurate description of the nocturnal boundary layer chemistry would require modeling of horizontal and vertical transport, i.e., altitude-resolved information (Geyer and Stutz, 2004). Such information was not available in this work.

The reactions used in this model are summarized in Table S-2. The mechanism consists of O_3 and NO_2 dry deposition, titration of NO with O_3 (R8) and chemical loss of O_3 to a generic biogenic hydrocarbon. For dry deposition, the velocities of $v_d(O_3)$ = 0.2 cm s^{-1} and $v_d(NO_2)$ = $\alpha \times v_d(O_3)$ with α=0.65 from Lin et al. (2010) were used. The rate constants for reaction with the generic biogenic hydrocarbon was set to that of α-pinene with O_3 (5×10^{-11} cm^3 $molec.^{-1}$ s^{-1}, (Seinfeld and Pandis, 2006)).

Model simulations were carried out using a custom differential equation integrator macro in the software package Igor Pro (Wavemetrics) and were initiated with the campaign median NO_2 and O_3 concentrations observed at sunset.

Table S-2. Reactions included in box model to estimate dry deposition velocities

Reaction	Rate constant
$O_3 \rightarrow$ products	$k_{dep}(O_3)$
$NO_2 \rightarrow$ products	$k_{dep}(NO_2)$
$O_3 + NO \rightarrow NO_2 + O_2$	4.8×10^{-4} $ppbv^{-1}$ s^{-1}
O_3 + VOC $\rightarrow$ products	1.25 $ppbv^{-1}$ s^{-1}

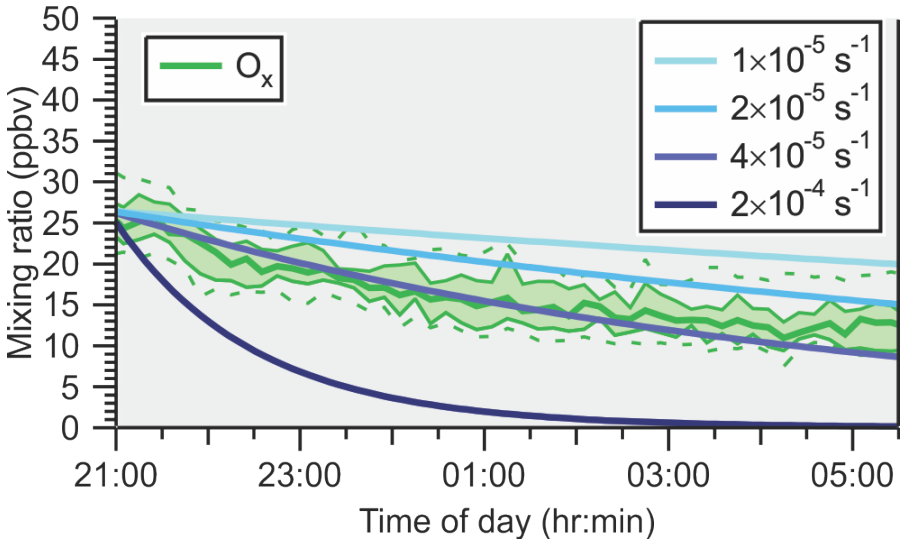

Figure S-2. Observed and simulated O_x loss in the NBL at Abbotsford assuming O_3 dry deposition rates of 2×10^{-4} s^{-1}, 4×10^{-5} s^{-1}, 2×10^{-5} s^{-1} and 1×10^{-5} s^{-1}, corresponding to approximate mixing heights of 10 m, 50 m, 100 m, and 200 m.

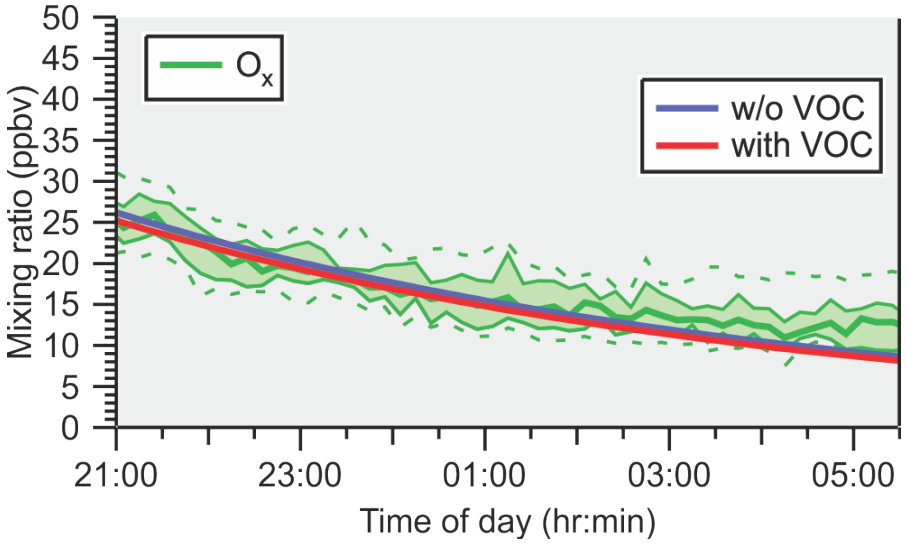

Figure S-3. Effect of biogenic VOC emissions on O_x. The observed and simulated O_x loss in the NBL at Abbotsford assuming an O_3 dry deposition rate of 4×10^{-5} s^{-1} are shown as green and blue traces, respectively. The red trace shows the effect of adding 1 ppbv of reactive biogenic VOC at sunset and continuous biogenic VOC emissions of 3×10^{5} molecules cm^{-3} s^{-1} throughout the night.

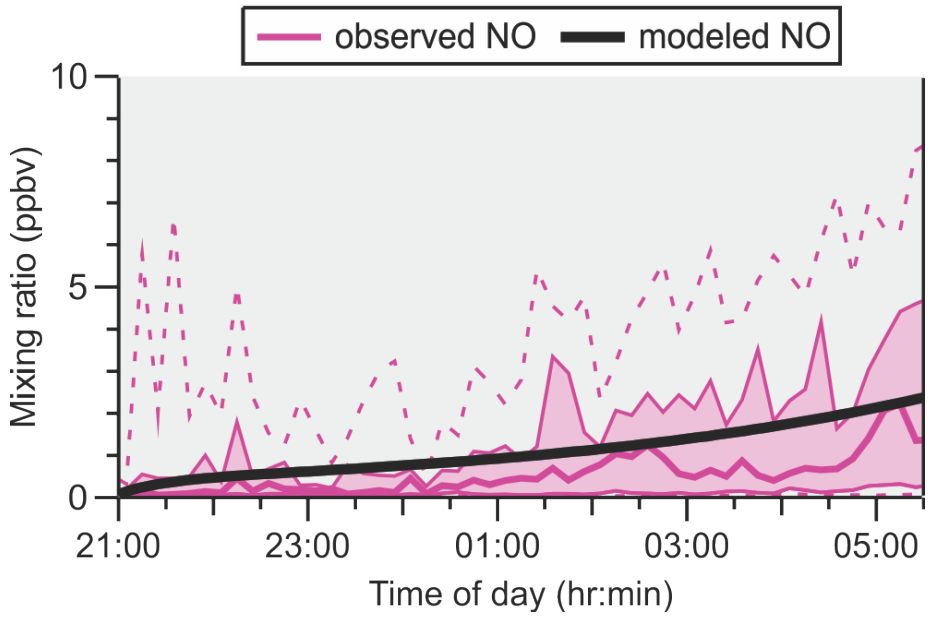

Figure S-4. Comparison of observed and simulated NO mixing ratios after constant emissions of 2.9×10^{-4} ppbv s^{-1} (~1.05 ppbv hr^{-1}) of NO and 3×10^{-5} ppbv s^{-1} (~0.05 ppbv hr^{-1}) of NO_2 were added.

Box model to determine the time necessary for NO_3 and N_2O_5 to achieve a steady state with respect to production and losses

The validity of the steady state assumption was evaluated in a similar fashion as described by Brown et al. (2003) using a simple box model. Reactions and rate coefficients included in these simulations are listed in Table S-3. Model simulations were carried out using a custom differential equation integrator macro in the software package Igor Pro (Wavemetrics). Rate coefficients were calculated for a temperature of 286 K, which is the median nocturnal temperature of this study (Figure 8B). Simulations were initiated with the median nocturnal NO_2 and O_3 mixing ratios of 7.5 ppbv (1.92×10^{11} molecules cm^{-3}) and of either 18 ppbv (4.5×10^{11} molecules cm^{-3}) or 5.0 ppbv (1.3×10^{11} molecules cm^{-3}), respectively. The simulations assume pseudo-first order N_2O_5 and NO_3 loss with frequencies of 1×10^{-3} s^{-1} and between 1×10^{-2} s^{-1} and 0 s^{-1}, respectively.

Simulated temporal profiles of NO_3 and N_2O_5 are show in Figure S-5 (left axis) and those of O_3 and NO2 on the right axis. The subpanels A, B, and C are simulations with k_{NO3} = 0 s^{-1}, 1×10^{-3} s^{-1} or 1×10^{-2} s^{-1}, respectively. In each case, the rate of change of $[N_2O_5]$ with respect to time, $d[N_2O_5]/dt$, approaches zero after a period of ~70 min, or less, indicating the time to approach steady state. The simulations also show that the amount of O_3 and NO_2 removed through chemical reactions of NO_3 and N_2O_5 are ~1 ppbv and between ~1.9 and ~1.6 ppbv over a period of 4 hours. These are upper limits as in this study much of the NO_3 was titrated by NO. In any case, loss of O_3 through nocturnal gas-phase is predicted to be rather small compared to the total O_3 loss observed (~26 ppbv over 9 hours, see section 3.1.3 and Figure 4C in the main text). Brown et al. (2003) show that in these scenarios, NO_3, N_2O_5, and NO_2 remain in equilibrium almost throughout; for completeness, the corresponding plot for these simulations is shown in Figure S-6.

As shown in equation (2) of the manuscript, the steady state lifetime is approximately equal to:

$$\frac{[N_2O_5]}{k_1[NO_2][O_3]} \approx \left(k_{N_2O_5} + \frac{k_{NO_3}}{K_2[NO_2]}\right)^{-1} \quad (2)$$

A comparison of these two expressions is shown in Figure S-7. The time when these two expressions are equal is equal to the time to steady state.

Table S-3. Reactions included in the box model to estimate the time for NO_3 and N_2O_5 to achieve steady state with respect to their production and loss

#	Reaction	Rate coefficient
R1	$NO_2 + O_3 \rightarrow NO_3 + O_2$	2.28×10^{-17} cm^3 molecule^{-1} s^{-1}
$R2_f$	$NO_3 + NO_2 \rightarrow N_2O_5$	1.35×10^{-12} cm^3 molecule^{-1} s^{-1}
$R2_r$	$N_2O_5 \rightarrow NO_3 + NO_2$	0.00923 s^{-1}
(R7)	$NO_3 \rightarrow$ products	$k_x = k_{NO3} = 0$ s^{-1}, 1×10^{-3} s^{-1} or 1×10^{-2} s^{-1}
(R5)	$N_2O_5 \rightarrow$ products	$k_y = k_{N2O5} = 1\times10^{-3}$ s^{-1}

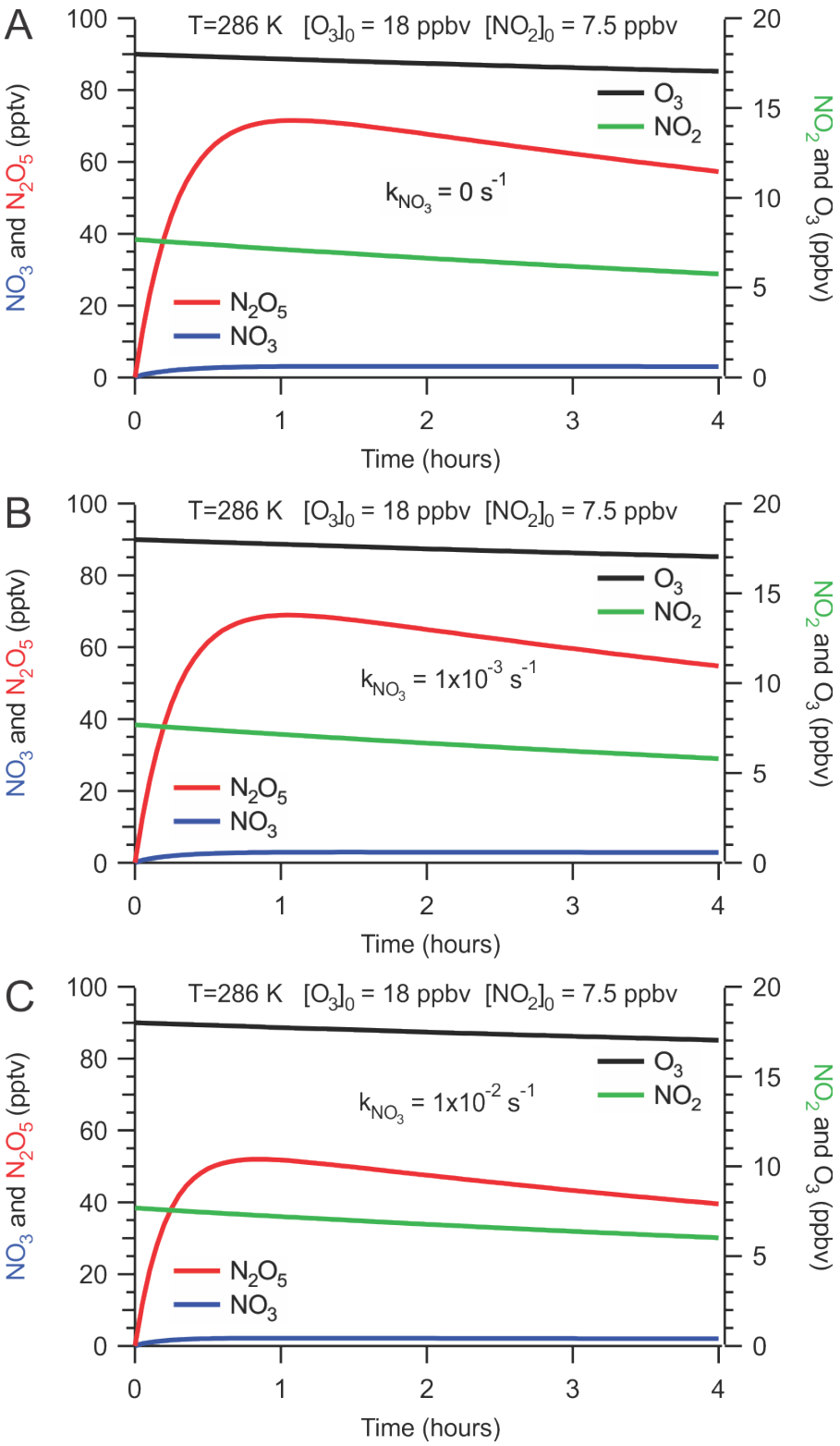

Figure S-5. Simulated temporal profiles of NO_3 and N_2O_5 (left axis) and O_3 and NO_2 (right axis). The subpanels A, B, and C are simulations with k_{NO3} = 0 s^{-1}, 1×10^{-3} s^{-1} or 1×10^{-2} s^{-1}, respectively.

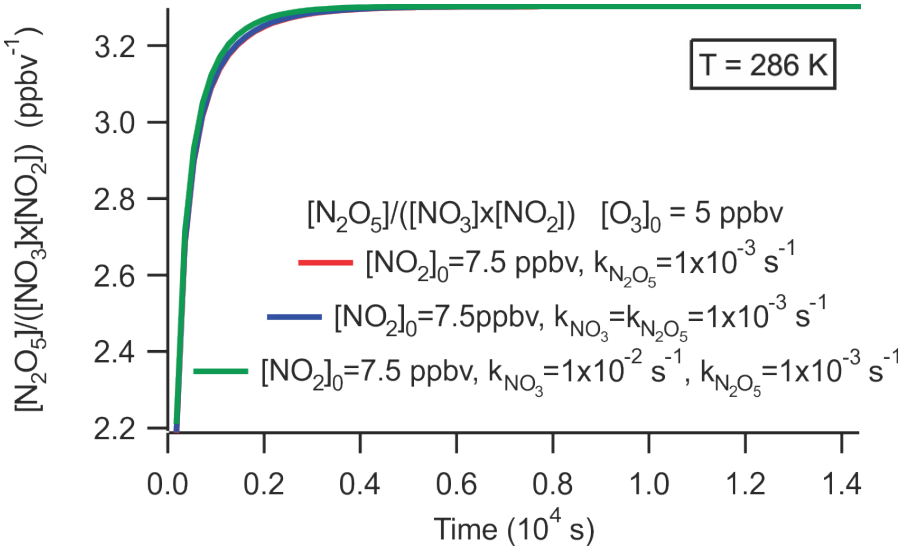

115

116 **Figure S-6**. Equilibrium constants for reaction (2) calculated for the three scenarios shown in

117 Figure S-5.

118

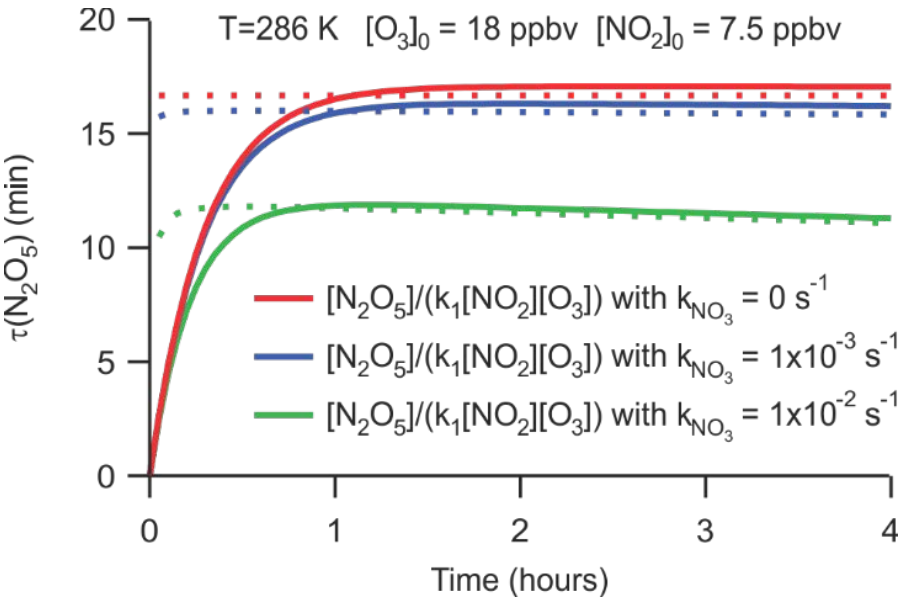

119

120 **Figure S-7**. Comparison of $\tau(N_2O_5)$ calculated using equation (2) of the main manuscript. with

121 the dashed lines calculated using equation (11) of Brown et al. (2003).

122

Estimates of how loss of NO_3 to VOCs would affect the lifetime of N_2O_5

The steady state lifetime calculation presented in Figure 8C of the main manuscript neglects losses of NO_3 to VOCs due to poor data coverage, i.e., presents a scenario where $\Sigma k_{NO3+VOC,i}[VOC]_i$ is assumed to be zero, which is, of course, unrealistic.

We used all available VOC data and calculated a time series of $\Sigma k_{NO3+VOC,i}[VOC]_i$. The average (±1 σ) value at night is (0.038±0.026) s^{-1}. The N_2O_5 loss frequency, calculated by dividing this value with the N_2O_5:NO_3 ratio, is (1.1±0.9)×10^{-5} s^{-1}, corresponding to a lifetime of ~2.5 hours, which is negligible.

However, as stated in the main manuscript, the VOC data coverage is sparse and did not include measurements of all hydrocarbons towards which NO_3 is reactive. Recently, Liebmann et al. (2018) reported an average of nocturnal NO_3 loss frequency of 0.11 s^{-1} in the boreal forest of Finland. This value likely included loss of NO_3 to NO and a variety of hydrocarbons such as sesqui- and diterpenes, which are likely present in higher concentration in a boreal forest than at Abbotsford and hence represents an upper limit Taking this value and dividing it by the N_2O_5:NO_3 ratio, the average nocturnal N_2O_5 loss frequency via NO_3-VOC reactions is calculated to (5.6±1.3)×10^{-3} s^{-1}. Figure S-8 shows the result of including this value in the calculation of N_2O_5 lifetime.

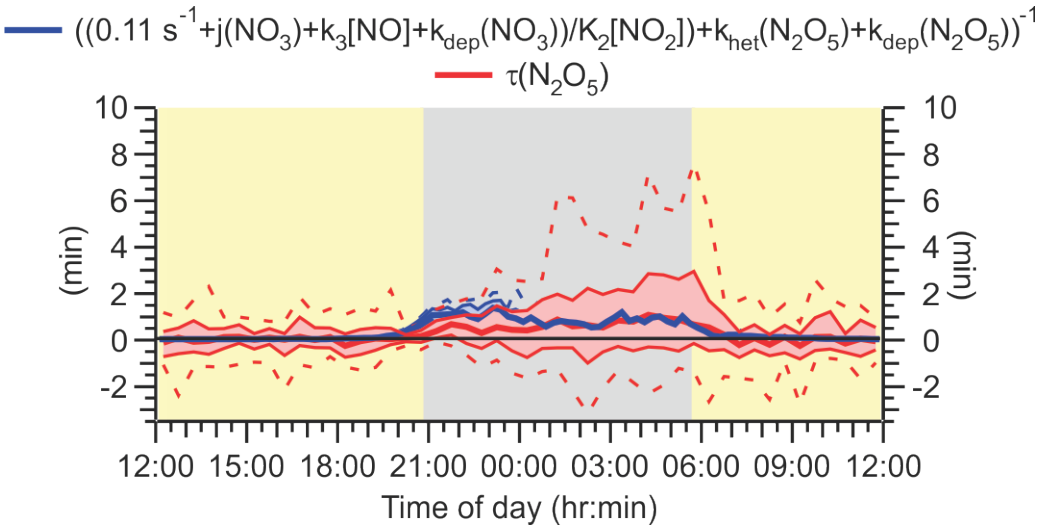

Figure S-8. Same as Figure 8c but including an assumed NO_3 loss frequency to VOCs of 0.11 s^{-1}.

References

Brown, S. S., Stark, H., and Ravishankara, A. R.: Applicability of the steady state approximation to the interpretation of atmospheric observations of NO_3 and N_2O_5, J. Geophys. Res., 108, 4539, 10.1029/2003JD003407, 2003.

Geyer, A., and Stutz, J.: Vertical profiles of NO_3, N_2O_5, O_3, and NO_x in the nocturnal boundary layer: 2. Model studies on the altitude dependence of composition and chemistry, J. Geophys. Res., 109, D12307, doi:12310.11029/12003JD004211, 2004.

Liebmann, J., Karu, E., Sobanski, N., Schuladen, J., Ehn, M., Schallhart, S., Quéléver, L., Hellen, H., Hakola, H., Hoffmann, T., Williams, J., Fischer, H., Lelieveld, J., and Crowley, J. N.: Direct measurement of NO_3 radical reactivity in a boreal forest, Atmos. Chem. Phys., 18, 3799-3815, 10.5194/acp-18-3799-2018, 2018.

Lin, C. H., Lai, C. H., Wu, Y. L., and Chen, M. J.: Simple model for estimating dry deposition velocity of ozone and its destruction in a polluted nocturnal boundary layer, Atmos. Environm., 44, 4364-4371, 10.1016/j.atmosenv.2010.07.053, 2010.

Seinfeld, J. H., and Pandis, S. N.: Atmospheric chemistry and physics: from air pollution to climate change, 2nd ed., Wiley, Hoboken, N.J., 2006.